ACS MATERIALS LETTERS

www.acsmaterialsletters.org

Intelligent Design of Artesunate-like Analogue Nanoassemblies for Optimized Antitumor Efficacy

Yulu Song,[#] Jianbin Shi,[#] Jiaqi Liang,[#] Xinyang Luo, Yutong Zhang, Jing Li,* Zhonggui He,* and Shenwu Zhang*

Cite This: *ACS Materials Lett.* 2026, 8, 249−257

Read Online

ACCESS | Metrics & More | Article Recommendations | Supporting Information

ABSTRACT: **Artemisinin derivatives show antitumor potential via their peroxide bridge, but dihydroartemisinin (DHA) suffers from poor solubility and limited targeting. In this study, inspired by artesunate (ART), we synthesized two derivatives, DHA-CC and DHA-SS, and prepared their PEGylated nanoassemblies (pNAs) using DSPE-PEG$_{2K}$ to enhance their *in vivo* stability and prolong circulation. Between the two derivatives, DHA-SS pNAs, with their unique disulfide bond structure, demonstrated superior stability, circulation time, and tumor accumulation. Importantly, DHA-SS pNAs exhibited specific responsive drug release under the reductive tumor microenvironment (TME), thereby achieving a favorable balance between systemic stability and efficient activation at the tumor site. *In vitro* and *in vivo* evaluations demonstrated that DHA-SS pNAs have higher reactive oxygen species (ROS) generation, greater cytotoxicity, and enhanced antitumor effects without evident systemic toxicity. Overall, these findings demonstrate that this rational structural modification offers a promising strategy for advancing artemisinin-based antitumor therapies toward clinical translation.**

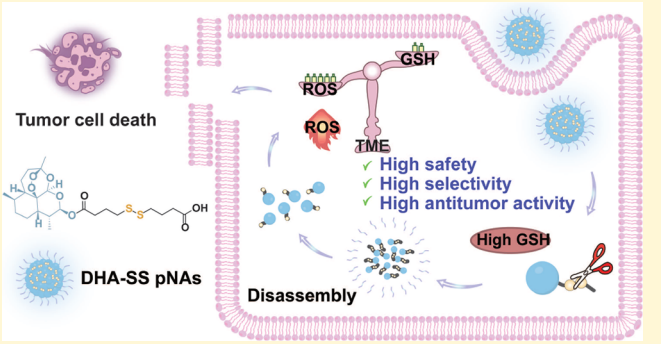

Cancer remains one of the leading causes of mortality worldwide, with both incidence and death rates continuing to rise. Despite advances in treatment, it poses a substantial threat to global public health.[1−3] Conventional chemotherapeutic agents are limited by poor tumor targeting, high systemic toxicity, and the frequent development of drug resistance.[4−6] Although novel modalities such as targeted therapy and immunotherapy have demonstrated remarkable clinical progress, challenges, including systemic adverse effects, therapeutic resistance, and tumor recurrence persist.[7] Consequently, structural optimization and dosage-form innovation of existing agents to develop efficient and low-toxicity treatment strategies remain important directions in cancer research.[8,9] In recent years, the antitumor potential of artemisinin and its derivatives, including dihydroartemisinin (DHA) and artesunate (ART), has attracted increasing attention.[10,11] Their activity is primarily attributed to the unique endoperoxide bridge within the molecular structure, which undergoes Fenton-like reactions catalyzed by high-concentration Fe^{2+} in the tumor microenvironment (TME), leading to the generation of reactive oxygen species (ROS) and oxidative stress-induced tumor cell death.[12] Despite these promising mechanisms, the clinical application of artemisinin-based drugs is constrained by pharmacokinetic and physicochemical limitations.[13] The representative derivative DHA exhibits extremely poor aqueous solubility and undergoes rapid metabolism *in vivo*, resulting in low bioavailability and diminished therapeutic efficacy. ART, through the introduction of a succinate monoester group, improves water solubility but still suffers from limited tumor targeting and suboptimal intratumoral accumulation.[14] In response to these challenges, a variety of delivery strategies for artemisinin-based drugs have been investigated. For instance, encapsulation within nanocarriers like liposomes, polymeric micelles, and metal−organic frameworks (MOFs) has been employed to enhance their solubility and bioavailability.[15−18] Other approaches have

Received: October 21, 2025
Revised: December 8, 2025
Accepted: December 9, 2025
Published: December 15, 2025

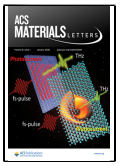

https://doi.org/10.1021/acsmaterialslett.5c01414
ACS Materials Lett. 2026, 8, 249−257

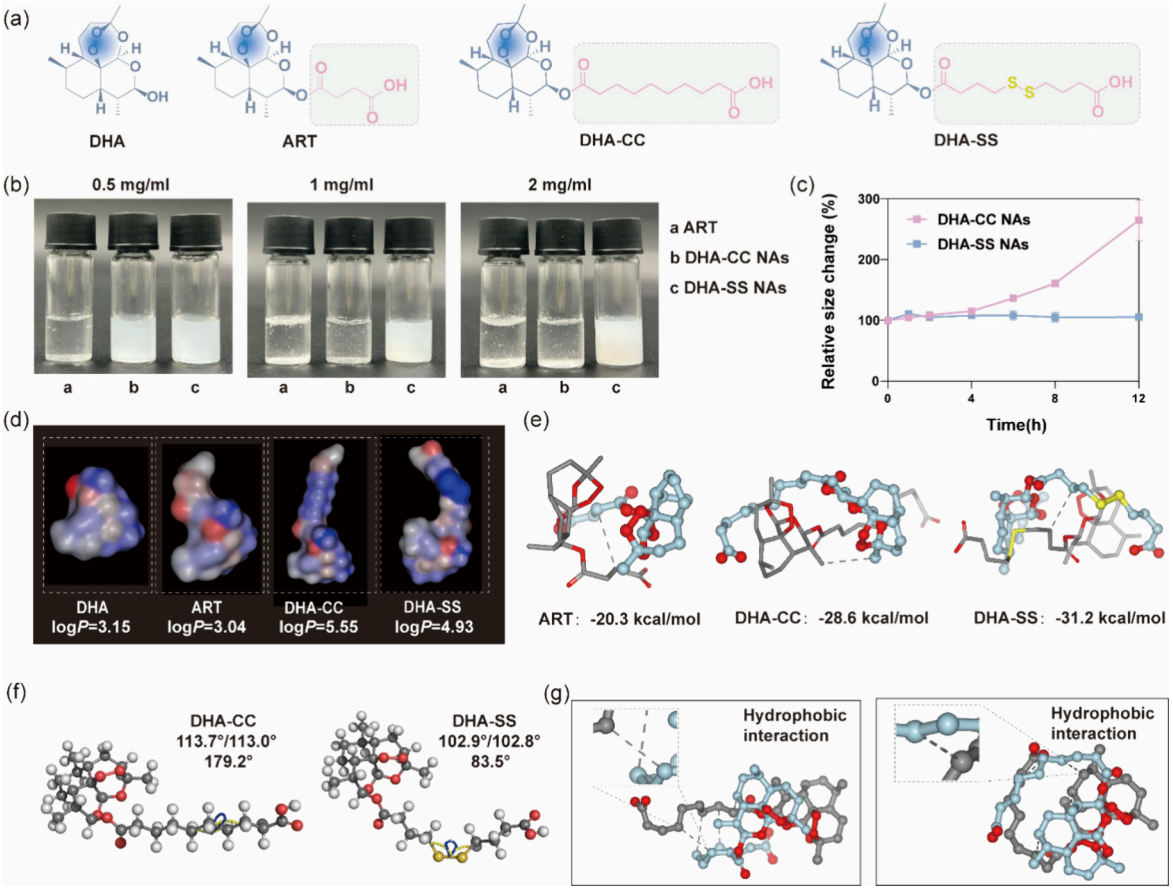

Figure 1. Structure−assembly relationship of DHA-R. (a) Precise structures of DHA, ART, DHA-CC, and DHA-SS. (b) Appearance of DHA-R NAs at different concentrations without the addition of DSPE-PEG$_{2K}$. (c) Stability of DHA-R NAs without the addition of DSPE-PEG$_{2K}$ in phosphate-buffered saline (PBS) (pH 7.4) mixed with 10% fetal bovine serum (FBS) (n = 3). (d) Log*P* of DHA, ART, DHA-CC, and DHA-SS. (e) Molecular docking and binding energies of ART, DHA-CC, and DHA-SS molecules. (f) Molecular simulation: bond angles and dihedral angles of −CC− in DHA-CC and −SS− in DHA-SS. (g) Simulation of the assembly mechanisms of the DHA-CC NAs and DHA-SS NAs.

included the construction of artemisinin dimers or their covalent conjugation to targeting moieties to improve stability and target specificit.[8] Nevertheless, these conventional, carrier-based strategies often face significant hurdles, such as poor drug-loading efficiency, burst release during circulation, complicated fabrication procedures, and carrier-associated biosafety issues.[19−21] Consequently, the development of a novel paradigm that allows for high drug loading, improved stability, and tumor-specific delivery is of critical importance for the clinical translation of these therapeutics.

Self-assembled nanoassemblies (NAs) have recently garnered attention as a novel delivery strategy. Unlike traditional nanocarriers, NAs leverage noncovalent interactions, such as hydrogen bonding, hydrophobic interactions, and $\pi-\pi$ stacking, enabling drug molecules themselves to self-assemble into NAs with high drug-loading efficiency.[22,23] This carrier-free approach effectively addresses compatibility and safety concerns associated with exogenous delivery systems. The success of this strategy depends on rational chemical modification of drug molecules, typically by introducing functional groups or side chains to confer amphiphilicity.[24] These modified molecules can spontaneously self-assemble in aqueous environments into NAs primarily composed of the drug itself.[25] Importantly, the chemical design not only dictates self-assembly behavior (morphology, size, stability) but also directly influences *in vivo* pharmacokinetics and targeting performance.[26]

Among various functional modifications, disulfide bonds represent a classic reduction-responsive moiety with unique advantages in tumor-targeted drug delivery.[27,28] The TME is characterized by a significantly elevated concentration of glutathione (GSH).[29] Specifically, the GSH level in tumor tissues is at least 4-fold higher than that in normal tissues. Drug delivery systems incorporating disulfide linkages exhibit stability in the extracellular environment and systemic circulation, yet undergo rapid cleavage upon cellular internalization within the reductive TME, thereby enabling triggered drug release or nanostructure disassembly.[30,31] This reduction-sensitive property renders disulfide bonds an ideal molecular switch for controlled tumor-specific drug release.[32] Beyond reduction-responsivity, disulfide bonds also impart unique structural features that influence molecular self-assembly.[33] With a bond angle and dihedral angle approaching 90°, disulfide linkages introduce steric hindrance and molecular rigidity, disrupting linear symmetry and promoting more compact molecular packing. Such conformational constraints can enhance hydrophobic interactions and $\pi-\pi$ stacking, thereby improving the stability, uniformity, and colloidal performance of NAs.[34] Compared with the flexible C−C single bonds, the moderate rigidity conferred by the disulfide

https://doi.org/10.1021/acsmaterialslett.5c01414
ACS Materials Lett. 2026, 8, 249−257

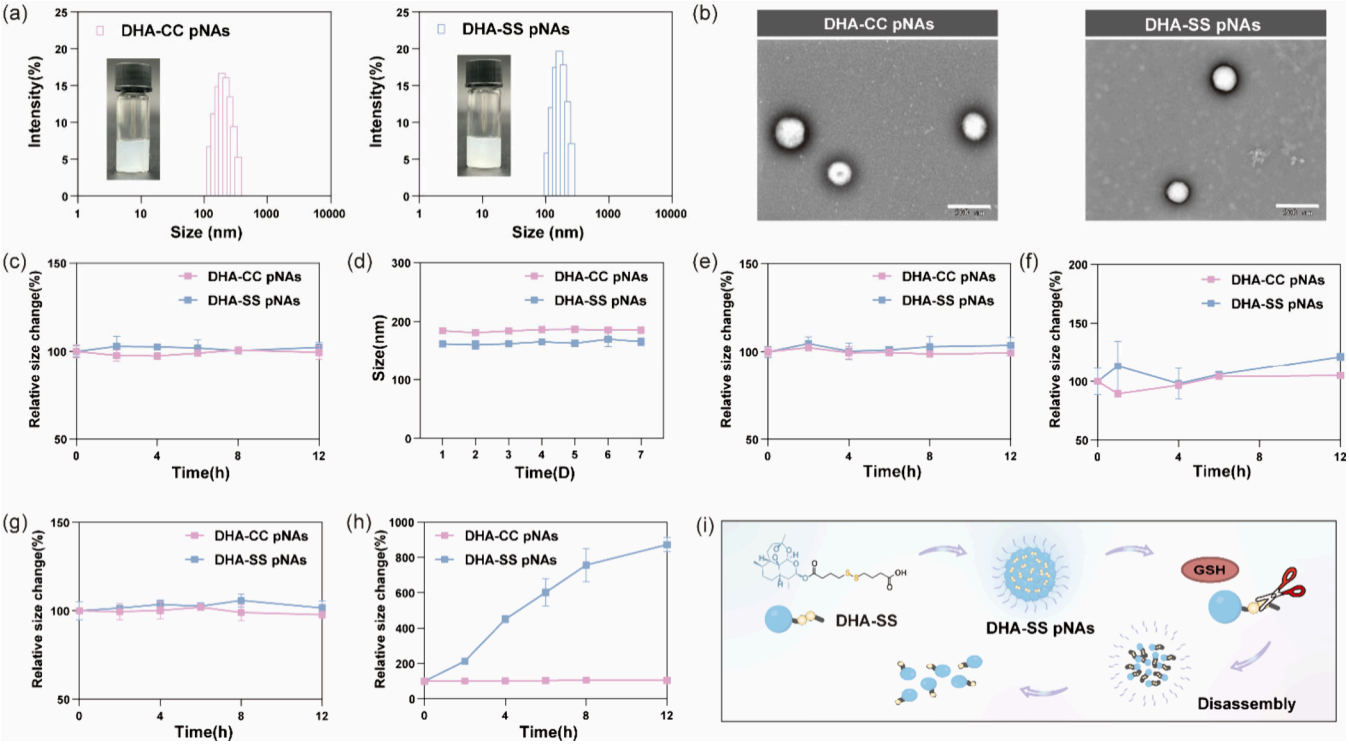

Figure 2. Characterization, stability, and reduction response comparison of DHA-R pNAs. (a) Particle size distribution profiles of DHA-CC pNAs and DHA-SS pNAs. (b) Transmission electron microscope (TEM) images of DHA-CC pNAs and DHA-SS pNAs. The scale bars correspond to 200 nm. (c) Stability of DHA-CC pNAs and DHA-SS pNAs at room temperature (n = 3). (d) Stability of DHA-CC pNAs and DHA-SS pNAs at 4 °C (n = 3). (e) Stability of DHA-CC pNAs and DHA-SS pNAs in PBS (pH 7.4) (n = 3). (f) Stability of DHA-CC pNAs and DHA-SS pNAs in PBS (pH 7.4) mixed with 10% FBS (n = 3). (g, h) Relative particle size of DHA-CC pNAs and DHA-SS pNAs in 0 mM dithiothreitol (DTT) and 10 mM DTT environments (n = 3). (i) Reduction-responsive mechanism of the disulfide bond. Data are presented as mean ± SD.

bonds effectively suppresses excessive molecular motion, yielding more stable NAs.[35]

Building upon the clinically validated structural design of ART, which successfully improved the solubility of DHA via succinic acid modification, this study proposed the rational design and synthesis of two novel DHA derivatives: DHA-CC, incorporating sebacic acid side chains, and DHA-SS, incorporating disulfide bond−containing side chains. Both derivatives were formulated into self-assembled NAs and subsequently modified with DSPE-PEG_{2K} to enhance systemic stability and prolong circulation time. By systematically comparing their self-assembly behavior, colloidal stability, pharmacokinetic profiles, *in vitro* antitumor activity, and *in vivo* therapeutic efficacy, this work aimed to elucidate the role of disulfide bond modification in enhancing the therapeutic performance of artemisinin derivatives. This study was designed to provide a potential antitumor candidate with translational potential, as well as to contribute to the ongoing development of structural optimization and delivery system strategies for clinically approved drugs.

To address the limitations of artemisinin derivatives, inspired by the structural design of ART, two DHA derivatives were synthesized via the pathway illustrated (Figures 1a and S1). These derivatives retain the essential peroxide pharmacophore, while incorporating a longer-chain sebacic acid in place of succinic acid and introducing a disulfide bond. Such structural modifications were intended to enhance molecular self-assembly and enable drug release in response to the TME. The chemical structures and purity of these synthesized compounds were confirmed by mass spectrometry (MS) and proton nuclear magnetic resonance (^{1}H NMR) (Figures S2−S5).

The self-assembly behavior of ART and DHA derivatives at different concentrations was investigated using a one-step nanoprecipitation method. DHA-SS formed uniform and stable NAs across all tested concentrations, indicating that the self-assembly capacity followed the order: DHA-SS > DHA-CC > ART. Furthermore, we evaluated the stability of two DHA derivatives NAs in PBS (pH 7.4) containing 10% FBS (Figure 1c). DHA-CC NAs disintegrated within 4 h, whereas DHA-SS NAs remained stable for 12 h, further confirming the superior self-assembly capacity of DHA-SS compared with DHA-CC.

The introduction of side chains increased the hydrophobicity of the molecules. The log$P$ values were shown in Figure 1d. As log$P$ is generally regarded as a key determinant of self-assembly behavior, the theoretical order of self-assembly ability based on hydrophobicity alone should be DHA-CC > DHA-SS > ART. However, this prediction did not align with the experimental results. These findings indicated that hydrophobicity was not the primary factor driving the superior self-assembly of DHA-SS. To elucidate the mechanism underlying the superior self-assembly behavior of DHA-SS compared with DHA-CC, molecular docking was first employed to calculate the binding energies of the respective molecules. The calculated binding energy of DHA-SS (−31.2 kcal/mol) was significantly lower than that of DHA-CC (−28.6 kcal/mol) and ART (−20.3 kcal/mol), indicating the strongest molecular interaction (Figure 1e). This theoretical

https://doi.org/10.1021/acsmaterialslett.5c01414
ACS Materials Lett. 2026, 8, 249−257

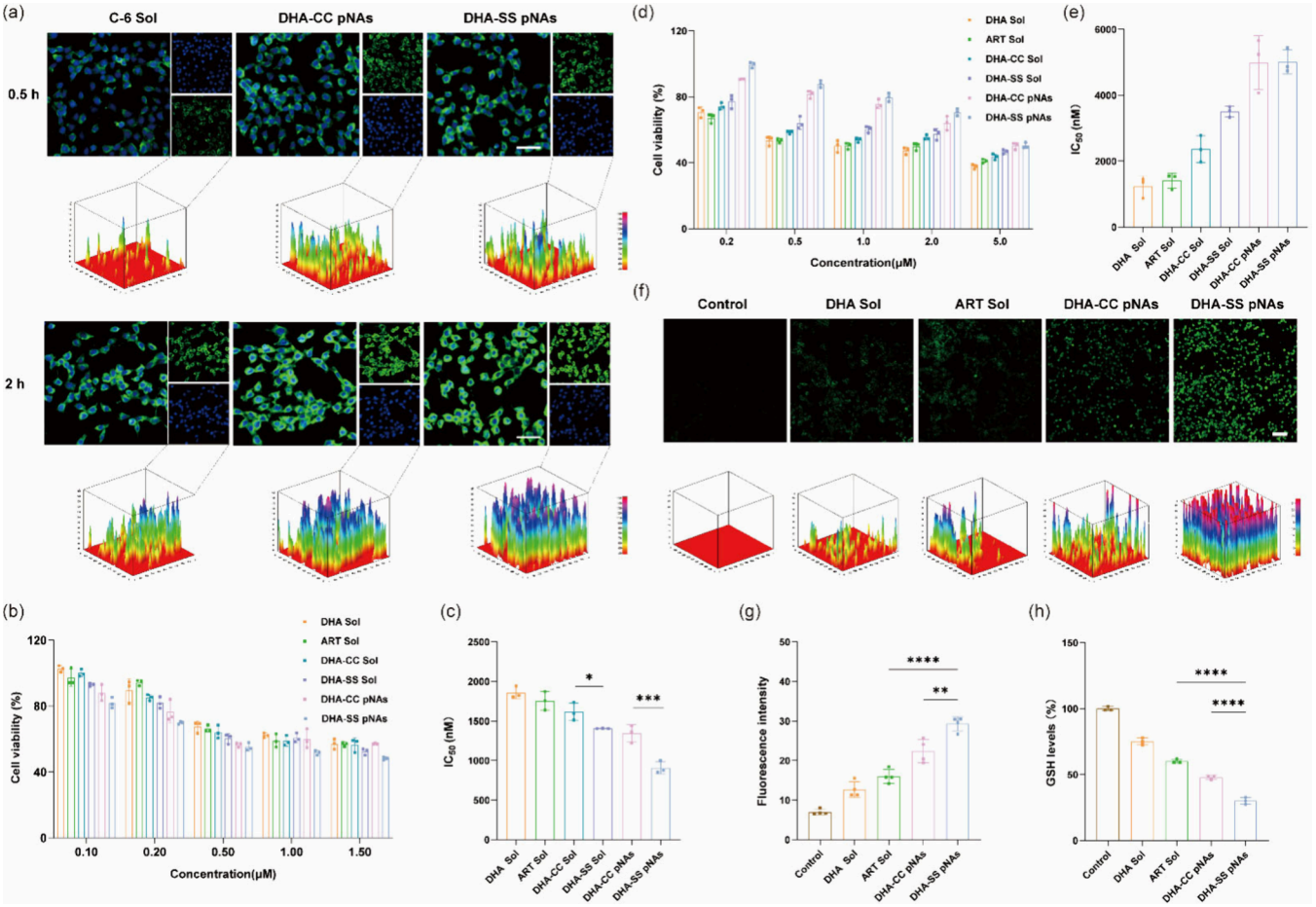

Figure 3. ***In vitro*** **antitumor activity and mechanism. (a) CLSM images of cellular uptake in 4T1 cells at 0.5 and 4 h, respectively. The scale bars correspond to 50 μm. (b) Cytotoxicity of different formulations against 4T1 cells for 48 h (n = 3). (c) IC_{50} values of different formulations on 4T1 cells (n = 3). (d) Cytotoxicity of different formulations against 3T3 cells for 48 h (n = 3). (e) IC_{50} values of different formulations on 3T3 cells (n = 3). (f) CLSM images and three-dimensional surface plot images analyzed by ImageJ showing ROS generation in 4T1 cells after 4 h of exposure to DHA-R pNAs. The scale bars correspond to 100 μm. (g) Quantitative analysis of ROS production in 4T1 cells by ImageJ (n = 4). (h) Intratumor content of GSH treated with different formulations (n = 3). Data are presented as mean ± SD. *p < 0.05, **p < 0.01, ***p < 0.001, ****p < 0.0001.**

result was highly consistent with the experimentally observed self-assembly behavior, reflecting a clear structure−activity relationship. Specifically, the lowest binding energy of DHA-SS predicted stronger intermolecular forces from an energy perspective, directly corresponding to the experimentally optimal self-assembly performance. In the concentration gradient experiments, DHA-SS formed uniform and stable NAs at all tested concentrations, while DHA-CC, with a higher binding energy, aggregated at higher concentrations (Figure 1b). DHA-SS NAs also showed the best antidilution stability in PBS (pH 7.4) containing 10% FBS (Figure 1c).

It is worth noting that the only structural difference between DHA-SS and DHA-CC lies in the introduction of a disulfide bond structure in the former. Therefore, based on the above results, it can be inferred that the disulfide bond played a critical role in modulating both assembly performance and colloidal stability of the DHA derivatives NAs. Specifically, the bond angle/dihedral angle of disulfide bonds can confer enhanced spatial flexibility, thereby facilitating self-assembly and improving structural stability. The most stable conformation has been found to correspond to the bond angle/dihedral angle of 90°. Therefore, we used the Materials Studio software package to calculate the bond angles of the sulfur (S)/C bonds and the dihedral angles of C−CC−C and C−SS−C. The −SS− bond angle in DHA-SS (102.9°/102.8°) was smaller than the −CC− bond angle in DHA-CC (113.7°/113.0°), and was closer to the ideal 90° (Figure 1f). Similarly, significant differences were observed in the dihedral angles: the C−SS−C dihedral angle (83.5°) was much closer to 90° than C−CC−C (179.2°). This structural advantage may further promote DHA-SS molecules to adopt a spatial orientation conducive to self-assembly, thereby enhancing the colloidal stability of the nanoscale assembly.

To further elucidate the assembly driving force at the molecular level, we conducted in-depth studies on the assembly mechanism of DHA-R using molecular docking and nanoassembly disruption experiments (Figures 1g and S6). The simulation and experimental results jointly confirmed that hydrophobic interactions remained the main fundamental force driving the initial aggregation of DHA-R molecules. Although DHA-CC had a higher log$P$ value, its assembly stability was much lower than that of DHA-SS. This seemingly contradictory phenomenon precisely indicated that, based on the initial driving force provided by hydrophobic interactions, the structural rigidity imparted by disulfide bonds played a crucial "strengthening" role in forming ordered and stable

https://doi.org/10.1021/acsmaterialslett.5c01414
ACS Materials Lett. 2026, 8, 249−257

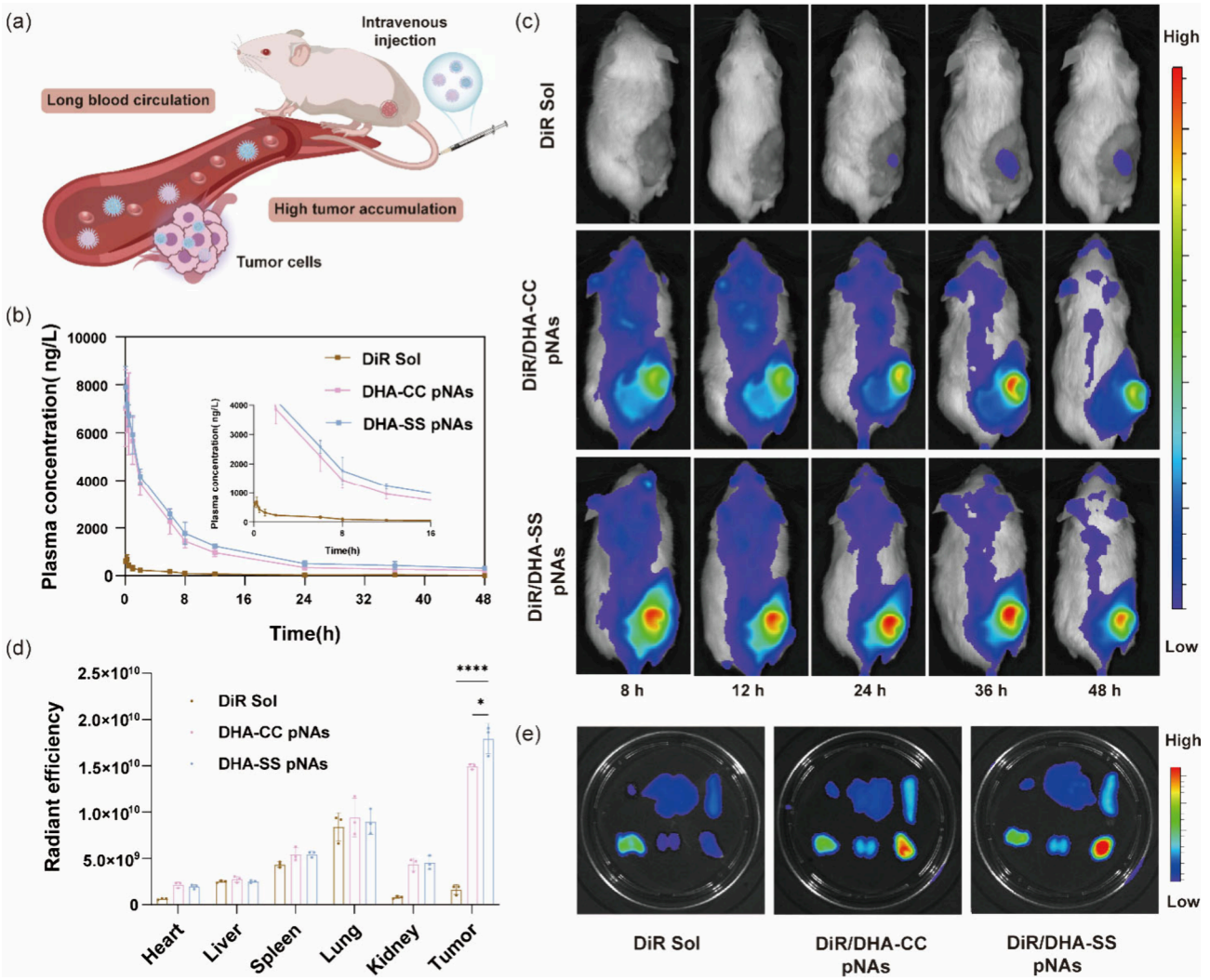

Figure 4. ***In vivo*** **pharmacokinetics and biodistribution study. (a) DHA-R pNAs in the bloodstream and at the tumor site. (b) Pharmacokinetic behavior of DHA-R pNAs *in vivo* (2 mg/kg, DiR equivalent) (n = 5). (c) *In vivo* fluorescence images of 4T1 tumor-bearing BALB/c mice at different time intervals (2 mg/kg, DiR equivalent). (d) Quantitative analysis of average fluorescence intensity of major organs and tumors at the brightest time point (2 mg/kg, DiR equivalent) (n = 3). (e) *In vitro* fluorescence images of major organs and tumors at the brightest time point (2 mg/kg, DiR equivalent) (n = 3). Data are presented as mean ± SD. *p < 0.05, ****p < 0.0001.**

advanced assembly structures. Therefore, the excellent self-assembly property of DHA-SS was attributed to the efficient synergy of the hydrophobic driving force and the structural stabilization mediated by the disulfide bonds.

In our previous study, non-PEGylated NAs were readily phagocytosed by the reticuloendothelial system (RES), leading to poor pharmacokinetic behavior and limited antitumor efficacy. To address this limitation, DSPE-PEG$_{2K}$ was introduced for PEGylation, aiming to prolong systemic circulation *in vivo*. The characterization results showed that the PEGylated NAs exhibited smaller particle sizes, uniform spherical morphologies, and comparable zeta potentials (Figures 2a,b and S7 and Table S1). Furthermore, energy-dispersive X-ray spectroscopy (EDX) revealed the composition of DHA-R pNAs (Figure S8). Remarkably, all DHA-R pNAs demonstrated superior drug-loading capabilities. A uniform drug loading of 80.0% (wt %) was achieved across all pNAs when DHA-R itself was considered the drug, a direct result of the constant mass ratio between DHA-R and the PEG modifier used during synthesis (Table S2). Furthermore, even when calculated based on the DHA as the drug, the pNAs maintained a substantial drug payload of at least 45.0% (Table S3).

Subsequently, we conducted a systematic assessment of the stability of DHA-R pNAs. Both formulations maintained their particle size during storage at room temperature and 4 °C (Figure 2c,d), as well as in PBS (pH 7.4) within 12 h (Figure 2e). Furthermore, they exhibited good stability in PBS (pH 7.4) containing 10% FBS (Figure 2f) and retained their original size after lyophilization and reconstitution (Figure S9). In summary, PEGylation markedly enhanced the stability of DHA-R pNAs. These improvements were of critical importance for extending systemic circulation, enhancing drug delivery efficiency, and ultimately improving antitumor efficacy *in vivo*.

The reduction-responsive disassembly of DHA-R pNAs was assessed by monitoring particle size changes in the presence and absence of DTT, a commonly used GSH analogue. While both pNAs remained stable in PBS alone, DHA-SS pNAs exhibited rapid size increase within 2 h under 10 mM DTT (Figure 2g,h), indicating reductive-triggered dissociation, which was further corroborated by TEM (Figure S10).

https://doi.org/10.1021/acsmaterialslett.5c01414
ACS Materials Lett. 2026, 8, 249−257

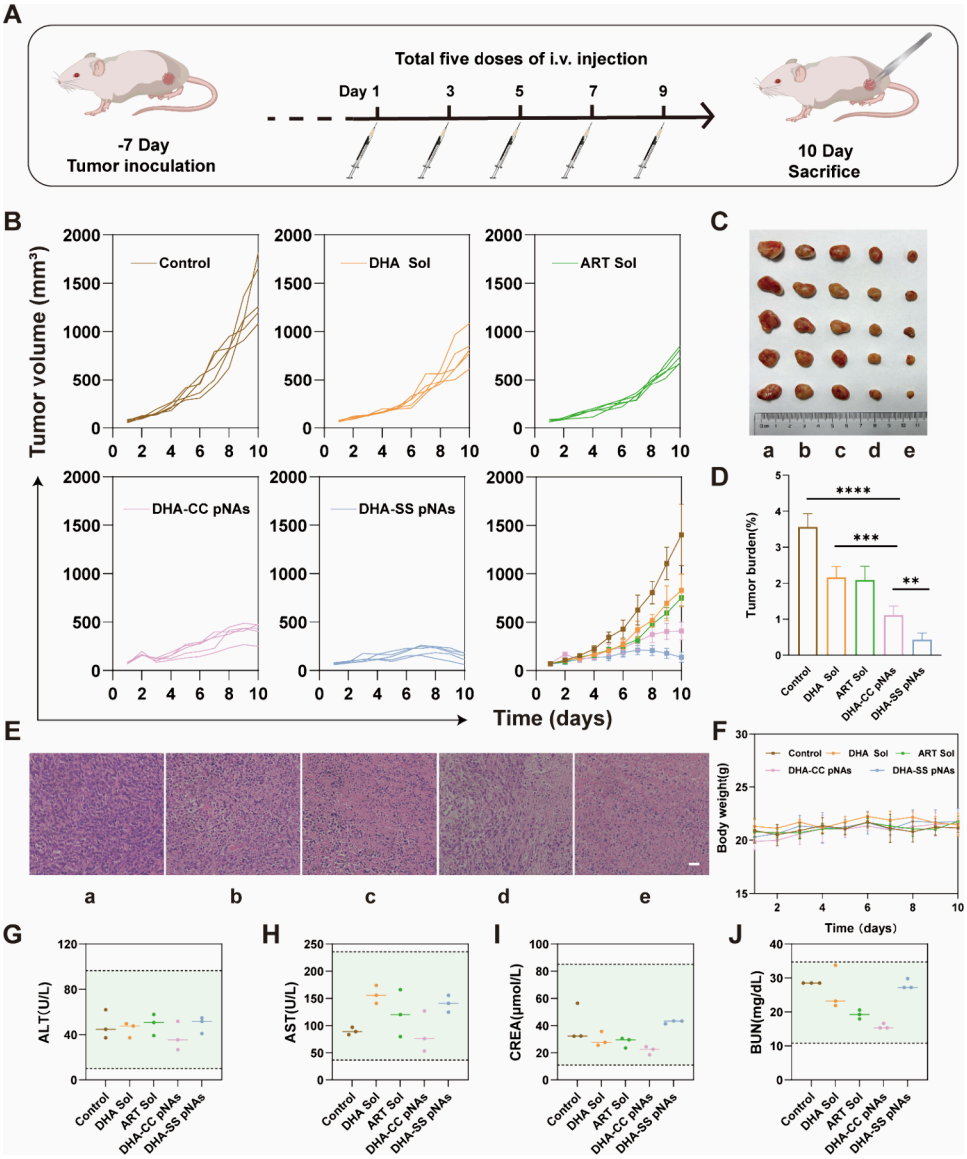

Figure 5. ***In vivo*** **evaluation of antitumor activity. (a) Schematic illustration of treatment schedule. (b) Tumor growth curves of 4T1 tumor-bearing BALB/c mice under different treatment regimens (10 mg/kg, ART equivalent) (*n* = 5). (c) Images of tumors after treatment (*n* = 5). (d) Comparison of tumor burden across different treatment groups (*n* = 5). (e) H&E staining images of tumor tissues. The scale bars correspond to 100 *μ*m. (f) Changes in mouse body weight during the treatment period (*n* = 5). (g, h) Liver function indicators during the treatment period (*n* = 3). (i, j) Kidney function indicators during the treatment period (*n* = 3). Data are presented as mean ± SD. **p* < 0.05, ***p* < 0.01, ****p* < 0.001, *****p* < 0.0001. a. Control, b. DHA Sol, c. ART Sol, d. DHA-CC pNAs, e. DHA-SS pNAs.**

Correspondingly, the release rate of DHA-SS pNAs reached approximately 60% within 8 h under 10 mM DTT (Figure S11). These results clearly indicated that the specific cleavage of disulfide bonds in DHA-SS pNAs led to the complete dissociation of the NAs, thus confirming their excellent reduction-responsive properties (Figure 2i).

Efficient cellular uptake is essential for pNAs to exert their antitumor effects. To assess this property, we investigated the uptake behavior of coumarin-6 (C-6)-labeled DHA-R pNAs using confocal laser scanning microscopy. Cells treated with DHA-R pNAs exhibited markedly stronger fluorescence signals compared with the C-6 solution (Sol) group under identical incubation conditions, indicating enhanced uptake efficiency of the nanoformulations (Figure 3a). Furthermore, the cellular uptake of pNAs exhibited a time-dependent manner.

We next compared the cytotoxic effects of different formulations on mouse breast cancer 4T1 cells (Figure 3b,c). Notably, DHA-SS pNAs achieved the highest cytotoxicity, which can be attributed to the synergistic effects of nanoscale delivery and the reductive activation of disulfide bonds, jointly facilitating efficient and selective drug release within tumor cells. To further evaluate biosafety, the cytotoxicity of DHA-R pNAs was examined in mouse embryonic fibroblast 3T3 cells and HC11 mammary epithelium.DHA-SS pNAs were less cytotoxic to 3T3 and HC11 cells than DHA-CC pNAs, indicating enhanced tumor selectivity (Figures 3d,e and S12).

Based on the cytotoxicity results described above, we further evaluated the ability of different formulations to induce ROS generation in 4T1 cells. In the DCFH-DA fluorescent probe assay, the group treated with DHA-SS pNAs displayed the most intense fluorescence, signifying a superior capacity for

https://doi.org/10.1021/acsmaterialslett.5c01414
ACS Materials Lett. 2026, 8, 249−257

ROS generation (Figure 3f,g). Flow cytometry further confirmed this observation (Figure S13). We further investigated the influence of drug treatment on the intracellular GSH levels. Treatment with DHA-SS pNAs resulted in the most pronounced reduction of intracellular GSH in 4T1 cells (Figure 3h). This observation was consistent with the ROS assay results, confirming that DHA-SS pNAs induce the strongest oxidative stress response.

The *in vivo* delivery efficiency of pNAs, particularly their pharmacokinetic behavior and tissue distribution, was a critical determinant of therapeutic efficacy. Therefore, we conducted pharmacokinetic studies in Sprague-Dawley rats by intravenously injecting different formulations, and systematically evaluated the blood retention and biodistribution (Figure 4a).

DiR Sol was rapidly cleared from systemic circulation, with its plasma concentration curve displaying a steep decline (Figure 4b and Table S4). In contrast, all DHA-R pNAs demonstrated markedly prolonged circulation times. These results confirmed that PEGylation significantly improved the stability of the nanodelivery system, thereby extending its blood retention and facilitating tumor site accumulation via the enhanced permeability and retention (EPR) effect. Notably, DHA-SS pNAs displayed the most favorable pharmacokinetic behavior among the tested groups, likely due to the additional structural stabilization conferred by disulfide bonding in combination with the protective PEG layer. This synergistic effect enabled DHA-SS pNAs to better evade systemic clearance, ultimately achieving more efficient tumor-targeted delivery.

To further evaluate the *in vivo* distribution characteristics and tumor-targeting ability of pNAs, we labeled DHA-R pNAs with the near-infrared fluorescent dye DiR and systematically studied their tissue distribution and tumor accumulation behavior in tumor-bearing mice. After injecting the same dose of DiR-labeled DHA-R pNAs or the free DiR Sol, the latter had a significantly lower overall fluorescence signal due to its poorer pharmacokinetic properties (Figure 4c). The DHA-R pNAs group reached the peak fluorescence intensity at 36 h and exhibited a longer retention time. This phenomenon can be attributed to the enhanced tumor aggregation achieved by the pNAs through the enhanced permeability and EPR effect.

To clarify the differences in the distribution of the pNAs in the main organs and tumors, we collected heart, liver, spleen, lung, kidney, and tumor tissues 36 h after injection (the peak fluorescence intensity time point), and compared their fluorescence intensities (Figure 4d,e). The results showed that DHA-SS pNAs showed significantly higher accumulation in the tumor site, which was consistent with the superior pharmacokinetic behavior of this group. These results indicated that the PEGylation modification not only significantly optimized the pharmacokinetic characteristics of DHA-R pNAs, but also improved their enrichment efficiency in the tumors through improving the biological distribution, thereby providing an *in vivo* distribution basis for its enhanced antitumor efficacy.

Based on the above favorable pharmacokinetic profile and tumor-targeting capability, DHA-R pNAs demonstrated marked therapeutic advantages, highlighting their potential as a promising anticancer nanomedicine. To further assess their *in vivo* efficacy, we systematically evaluated the antitumor activity of different formulations in a 4T1 tumor-bearing mouse model. Tumor-bearing mice were randomly assigned to groups and intravenously administered with different formulations (Figure 5a). Following the final administration, blood, major organs, and tumor tissues were collected for efficacy and safety assessment. Tumor volume and body weight were monitored daily throughout the treatment period.

Tumor growth inhibition was more pronounced in the pNAs-treated groups compared to the DHA and ART Sol groups (Figure 5b–e). Among these, DHA-SS pNAs achieved the most significant tumor suppression. This superior outcome can be attributed to multiple factors, including enhanced stability, improved cellular uptake, elevated cytotoxicity, and favorable *in vivo* pharmacokinetics.

The key mechanism study indicated that DHA-SS pNAs exhibited unique activation characteristics in the TME. Fluorescence imaging of ROS in tumor tissue sections (Figure S14) showed that the DHA-SS pNAs treatment group triggered the strongest ROS signal in the tumor area, indicating that it effectively triggered a Fenton-like reaction at the tumor site. At the same time, the results of intratumoral GSH level determination (Figure S15) showed that the GSH content in the tumor tissues of the DHA-SS pNAs treatment group was significantly reduced, which confirmed that the disulfide bond structure of DHA-SS pNAs was extensively reduced in tumor cells, while also consuming the key antioxidant substances in tumor cells, further intensifying oxidative stress. These findings collectively indicated that DHA-SS pNAs not only achieved tumor-targeted delivery through the EPR effect but also underwent specific activation within tumor cells. Through the dual effects of "ROS burst" and "GSH depletion", they effectively disrupted the redox balance of tumor cells, thereby generating a powerful antitumor effect.

Histological analysis further supported these findings. H&E staining of tumor tissues confirmed the marked tumor growth inhibition observed in the DHA-SS pNAs group (Figure 5e). Regarding safety, body weight in all treatment groups remained stable throughout the study, and no significant alterations were detected in liver and kidney function parameters following treatment (Figure 5f–j). Additionally, H&E staining of major organs revealed no observable pathological abnormalities, suggesting that DHA-R pNAs possess favorable biocompatibility and *in vivo* safety (Figure S16).

Inspired by the structure of the clinically used drug ART, this study constructed a self-assembling, reduction-responsive nanodrug, DHA-SS, through the precise structural modification of DHA while preserving its core pharmacophore, the peroxide bridge. From a molecular and structural perspective, the nearly 90° dihedral angle of the disulfide bond imparted suitable rigidity to the molecule, enhanced intermolecular interactions, and drove the efficient assembly of DHA-SS into structurally stable NAs. This structural advantage translated into superior macroscopic pharmacokinetic behaviors, including prolonged blood circulation and enhanced tumor-targeted accumulation. Functionally, the disulfide bond acted as an endogenous responsive switch that can be specifically activated by the high concentration of GSH within tumor cells, enabling controlled drug release and elegantly balancing the relationship between *in vivo* stability and therapeutic activation. In the 4T1 breast cancer animal model, DHA-SS pNAs demonstrated significant antitumor effects with no obvious systemic toxicity observed, indicating a broad therapeutic window. In conclusion, this research confirmed that the direct functionalization of DHA, based on structural inspiration from artemisinin-based drugs, was a highly effective strategy to

https://doi.org/10.1021/acsmaterialslett.5c01414
ACS Materials Lett. 2026, 8, 249–257

simultaneously improve its pharmacokinetic properties, tumor-targeting capability, and therapeutic index. The design and performance of DHA-SS pNAs support its further investigation as a potential artemisinin-based antitumor agent with translational promise.

■ ASSOCIATED CONTENT

Supporting Information

The Supporting Information is available free of charge at https://pubs.acs.org/doi/10.1021/acsmaterialslett.5c01414.

Materials and methods, synthetic route for DHA-R, mass spectra of DHA-R, ^{1}H NMR of DHA-R, particle size of DHA-R NAs treated with destructive agents (NaCl, SDS, and urea), zeta potential of DHA-R pNAs, EDS of DHA-R pNAs, lyophilization stability, TEM images showing the particle size distribution of DHA-R pNAs with DTT, *in vitro* drug release patterns of DHA-R pNAs, IC_{50} values of different formulations on HC11 cells, flow cytometric quantification of ROS in 4T1 treated with DHA-R pNAs, measurement of ROS generation using the DHE assay, intratumor content of GSH upon treatment with different formulations, H&E staining images of various organs under different treatments, characterization of DHA-R pNAs, drug loading rate of DHA-R and DHA in DHA-R pNAs, and pharmacokinetic parameters of SD rats after various treatments (PDF)

■ AUTHOR INFORMATION

Corresponding Authors

Jing Li − *School of Pharmacy, Shenyang Medical College, Shenyang 110034, P. R. China*; Email: dddefghijklmn@163.com

Zhonggui He − *Wuya College of Innovation and Joint International Research Laboratory of Intelligent Drug Delivery Systems of Ministry of Education, Shenyang Pharmaceutical University, Shenyang 110016, P. R. China*; Email: hezhonggui@vip.163.com

Shenwu Zhang − *Wuya College of Innovation, Shenyang Pharmaceutical University, Shenyang 110016, P. R. China*; orcid.org/0000-0001-5844-8957; Phone: +86-024-23986321; Email: zhangshenwu@syphu.edu.cn; Fax: +86-024-23986321

Authors

Yulu Song − *Wuya College of Innovation, Shenyang Pharmaceutical University, Shenyang 110016, P. R. China*

Jianbin Shi − *Wuya College of Innovation, Shenyang Pharmaceutical University, Shenyang 110016, P. R. China*

Jiaqi Liang − *Wuya College of Innovation, Shenyang Pharmaceutical University, Shenyang 110016, P. R. China*

Xinyang Luo − *College of Chemistry, Jilin University, Jilin 130000, P. R. China*

Yutong Zhang − *Wuya College of Innovation, Shenyang Pharmaceutical University, Shenyang 110016, P. R. China*

Complete contact information is available at: https://pubs.acs.org/10.1021/acsmaterialslett.5c01414

Author Contributions

#Y. Song, J. Shi, and J. Liang contributed equally to this work.

Notes

The authors declare no competing financial interest.

■ ACKNOWLEDGMENTS

This work was financially supported by the Department of Education of Liaoning Province (LJ212410163015), the Excellent Youth Science Foundation of Liaoning Province (2024JH3/10200046), the Liaoning Revitalization Talent Program (XLYC2403107), and the Shenyang Young and Middle-Aged Science and Technology Innovation Talent Support Program (RC240393).

■ REFERENCES

(1) Cao, W.; Qin, K.; Li, F.; Chen, W. Comparative Study of Cancer Profiles between 2020 and 2022 Using Global Cancer Statistics (GLOBOCAN). *J. Natl. Cancer Cent.* **2024**, *4*, 128−134.

(2) Wu, Z.; Xia, F.; Lin, R. Global Burden of Cancer and Associated Risk Factors in 204 Countries and Territories, 1980−2021: A Systematic Analysis for the GBD 2021. *J. Hematol. Oncol.* **2024**, *17*, No. 119.

(3) Editorial. The Global Challenge of Cancer. *Nat. Cancer* **2020**, *1*, 1−2.

(4) Koirala, M.; DiPaola, M. Overcoming Cancer Resistance: Strategies and Modalities for Effective Treatment. *Biomedicines* **2024**, *12*, No. 1801.

(5) Davodabadi, F.; Sajjadi, S. F.; Sarhadi, M.; Mirghasemi, S.; Nadali Hezaveh, M.; Khosravi, S.; Kamali Andani, M.; Cordani, M.; Basiri, M.; Ghavami, S. Cancer Chemotherapy Resistance: Mechanisms and Recent Breakthrough in Targeted Drug Delivery. *Eur. J. Pharmacol.* **2023**, *958*, No. 176013.

(6) Anand, U.; Dey, A.; Chandel, A. K. S.; Sanyal, R.; Mishra, A.; Pandey, D. K.; De Falco, V.; Upadhyay, A.; Kandimalla, R.; Chaudhary, A.; Dhanjal, J. K.; Dewanjee, S.; Vallamkondu, J.; Pérez de la Lastra, J. M. Cancer Chemotherapy and beyond: Current Status, Drug Candidates, Associated Risks and Progress in Targeted Therapeutics. *Genes Dis.* **2023**, *10*, 1367−1401.

(7) Liu, C.; Yang, M.; Zhang, D.; Chen, M.; Zhu, D. Clinical Cancer Immunotherapy: Current Progress and Prospects. *Front. Immunol.* **2022**, *13*, No. 961805.

(8) Du, Y.; Giannangelo, C.; He, W.; Shami, G. J.; Zhou, W.; Yang, T.; Creek, D. J.; Dogovski, C.; Li, X.; Tilley, L. Dimeric Artesunate Glycerophosphocholine Conjugate Nano-Assemblies as Slow-Release Antimalarials to Overcome Kelch 13 Mutant Artemisinin Resistance. *Antimicrob. Agents Chemother.* **2022**, *66*, No. e02065-21.

(9) Du, Y.; Li, C.; Zhang, Y.; Xiong, W.; Wang, F.; Wang, J.; Zhang, Y.; Deng, L.; Li, X.; Chen, W.; Cui, W. In Situ-Activated Phospholipid-Mimic Artemisinin Prodrug via Injectable Hydrogel Nano/Microsphere for Rheumatoid Arthritis Therapy. *Research* **2022**, *2022*, No. 0003.

(10) Dai, X.; Zhang, X.; Chen, W.; Chen, Y.; Zhang, Q.; Mo, S.; Lu, J. Dihydroartemisinin: A Potential Natural Anticancer Drug. *Int. J. Biol. Sci.* **2021**, *17*, 603−622.

(11) Addissouky, T. A. Artemisinin and Its Derivatives throughout the Therapeutic Mechanisms and Clinical Potential. *Discovery Chem.* **2025**, *2*, No. 10.

(12) Wang, J.; Xu, C.; Wong, Y. K.; Li, Y.; Liao, F.; Jiang, T.; Tu, Y. Artemisinin, the Magic Drug Discovered from Traditional Chinese Medicine. *Engineering* **2019**, *5*, 32−39.

(13) Huang, Y.; Yang, Y.; Liu, G.; Xu, M. New Clinical Application Prospects of Artemisinin and Its Derivatives: A Scoping Review. *Infect. Dis. Poverty* **2023**, *12*, No. 115.

(14) Osonwa, U. E.; Hu, M. Bioavailability and Pharmacokinetics of Dihydroartemisinin (DHA) and Its Analogs—Mechanistic Studies on Its ADME. *Curr. Pharm. Rep.* **2018**, *4*, 33−44.

(15) Shen, S.; Du, M.; Liu, Q.; Gao, P.; Wang, J.; Liu, S.; Gu, L. Development of GLUT1-Targeting Alkyl Glucoside-Modified Dihydroartemisinin Liposomes for Cancer Therapy. *Nanoscale* **2020**, *12*, 21901−21912.

(16) Liu, H.; Liu, Y.; Li, N.; Zhang, G.-Q.; Wang, M. Ginsenoside Rg_3 Based Liposomes Target Delivery of Dihydroartemisinin and

Paclitaxel for Treatment of Triple-Negative Breast Cancer. *Zhongguo Zhong Yao Za Zhi* **2023**, *48*, 3472−3484.
(17) Manjili, H. K.; Malvandi, H.; Mousavi, M. S.; Attari, E.; Danafar, H. In Vitro and in Vivo Delivery of Artemisinin Loaded PCL−PEG−PCL Micelles and Its Pharmacokinetic Study. *Artif. Cells, Nanomed., Biotechnol.* **2018**, *46*, 926−936.
(18) Yan, Y.; Yang, X.; Han, N.; Liu, Y.; Liang, Q.; Li, L.-G.; Hu, J.; Li, T.-F.; Xu, Z. Metal-Organic Framework-Encapsulated Dihydroartemisinin Nanoparticles Induces Apoptotic Cell Death in Ovarian Cancer by Blocking ROMO1-Mediated ROS Production. *J. Nanobiotechnol.* **2023**, *21*, No. 204.
(19) Sun, D.; Sun, X.; Shi, J.; Shi, X.; Sun, J.; Luo, C.; He, Z.; Zhang, S. Oxygen-Boosted Fluorinated Prodrug Hybrid Nanoassemblies for Bidirectional Amplification of Breast Cancer Ferroptosis. *J. Controlled Release* **2025**, *377*, 619−631.
(20) Yang, X.; Feng, C.; Wang, P.; Xie, S.; Wang, Y.; Zhang, H.; He, Z.; Zhang, S.; Luo, C. Precisely Self-cooperative Nanoassembly Enables Photothermal/Ferroptosis Synergistic Tumor Eradication. *Adv. Healthcare Mater.* **2024**, *13*, No. 2304485.
(21) Liu, Q.; Zou, J.; Chen, Z.; He, W.; Wu, W. Current Research Trends of Nanomedicines. *Acta Pharm. Sin. B* **2023**, *13*, 4391−4416.
(22) Wu, J.; Zhang, X.; Sun, D.; Shi, X.; Sun, J.; Luo, C.; He, Z.; Zhang, S. Molecularly Engineering a Lipid Nanoregulator Destroying the Last Defense of Ferroptosis in Breast Cancer Therapy. *Chem. Eng. J.* **2024**, *495*, No. 153366.
(23) Zhang, H.; Zhang, S.; Liu, S.; Fang, M.; Wang, Y.; Zhang, S.; Sun, J.; He, Z.; Luo, C. Self-Actuated Clot-Piercing Nanoassembly Enabling Adaptable Drug Activation and Synergistic Thrombus Ablation. *Adv. Funct Mater.* **2025**, *35*, No. 2416968.
(24) Liang, J.; Wu, J.; Shi, J.; Wen, S.; Zhang, Z.; Sun, J.; He, Z.; Luo, C.; Zhang, S. Fatty Chain Engineering Dictates Self-Assembly Behavior of Linker-Free Artesunate Nanoassemblies for Optimized Antitumor Efficacy. *Nano Res.* **2025**, *18*, No. 94907773.
(25) Wang, Y.; Sun, X.; Shi, J.; Zhang, Z.; Sun, J.; Luo, C.; He, Z.; Zhang, S. Chain Architecture-Engineered Artesunate Nanoassemblies Target LONP1 to Induce Oxidative Damage for Enhanced Anti-Tumor Therapy. *Chin. Chem. Lett.* **2026**, *37*, No. 111609.
(26) Wang, P.; Sun, X.; Feng, C.; Liu, S.; Chen, Q.; Zhang, S.; Sun, J.; He, Z.; Wang, Y.; Luo, C. Functional Artemisinin Derivative-Engineered Nanohybrids Boost Ferroptosis Stress-Driven Cancer Therapy. *Adv. Compos. Hybrid Mater.* **2025**, *8*, 315.
(27) Sun, B.; Luo, C.; Yu, H.; Zhang, X.; Chen, Q.; Yang, W.; Wang, M.; Kan, Q.; Zhang, H.; Wang, Y.; He, Z.; Sun, J. Disulfide Bond-Driven Oxidation- and Reduction-Responsive Prodrug Nanoassemblies for Cancer Therapy. *Nano Lett.* **2018**, *18*, 3643−3650.
(28) Wang, J.; Sun, X.; Mao, W.; Sun, W.; Tang, J.; Sui, M.; Shen, Y.; Gu, Z. Tumor Redox Heterogeneity-responsive Prodrug Nanocapsules for Cancer Chemotherapy. *Adv. Mater.* **2013**, *25*, 3670−3676.
(29) Wang, J.; Zhang, Q.; Li, Y.; Pan, X.; Shan, Y.; Zhang, J. Remodeling the Tumor Microenvironment by Vascular Normalization and GSH-Depletion for Augmenting Tumor Immunotherapy. *Chin. Chem. Lett.* **2024**, *35*, No. 108746.
(30) Ding, Y.; Dai, Y.; Wu, M.; Li, L. Glutathione-Mediated Nanomedicines for Cancer Diagnosis and Therapy. *Chem. Eng. J.* **2021**, *426*, No. 128880.
(31) Musa, M.; Sun, X.; Shi, J.; Li, J.; Zhang, S.; Shi, X. Differentially Engineered Nano-Tracker of Intracellular Drug for Potentiating Breast Cancer Treatment. *J. Colloid Interface Sci.* **2025**, *699*, No. 138199.
(32) Wei, J.; Qian, Y.; Bao, L.; Song, W.; Bi, Y. Disulfide Bonds as a Molecular Switch of Enzyme-Activatable Anticancer Drug Precise Release for Fluorescence Imaging and Enhancing Tumor Therapy. *Talanta* **2024**, *278*, No. 126394.
(33) Fu, S.; Rempson, C. M.; Puche, V.; Zhao, B.; Zhang, F. Construction of Disulfide Containing Redox-Responsive Polymeric Nanomedicine. *Methods* **2022**, *199*, 67−79.
(34) Li, L.; Liu, T.; Zuo, S.; Li, Y.; Zhao, E.; Lu, Q.; Wang, D.; Sun, Y.; He, Z.; Sun, B.; Sun, J. Satellite-type Sulfur Atom Distribution in Trithiocarbonate Bond-bridged Dimeric Prodrug Nanoassemblies: Achieving Both Stability and Activatability. *Adv. Mater.* **2024**, *36*, No. 2310633.
(35) Sun, B.; Luo, C.; Zhang, X.; Guo, M.; Sun, M.; Yu, H.; Chen, Q.; Yang, W.; Wang, M.; Zuo, S.; Chen, P.; Kan, Q.; Zhang, H.; Wang, Y.; He, Z.; Sun, J. Probing the Impact of Sulfur/Selenium/Carbon Linkages on Prodrug Nanoassemblies for Cancer Therapy. *Nat. Commun.* **2019**, *10*, No. 3211.

https://doi.org/10.1021/acsmaterialslett.5c01414
ACS Materials Lett. 2026, 8, 249−257